

# Overcoming a Solid Solution System on Chiral Resolution; Combining Crystallization and Enantioselective Dissolution

Ryusei Oketani,<sup>\*†</sup> Koki Shiohara,<sup>†</sup> Ichiro Hisaki<sup>\*</sup>

Division of Chemistry, Graduate School of Engineering Science, Osaka University  
1-3 Machikaneyama, Toyonaka, Osaka 560-8531, Japan.

<sup>†</sup>These authors are equally contributed to the work. All authors agreed to switch the order of the first and second authors in their personal CV.

<sup>\*</sup>Corresponding author: r.oketani.es@osaka-u.ac.jp (R.O.), i.hisaki.es@osaka-u.ac.jp (I.H.)

## Table of Contents

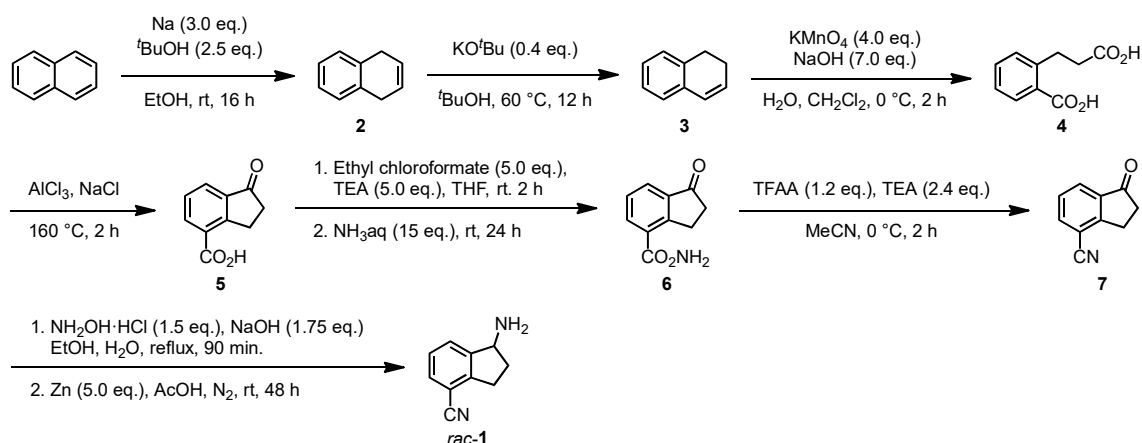
General	(page 2)
Synthesis of <i>rac</i> -4-cyano-1-aminoindane	(page 2)
Single crystal X-ray diffraction	(page 3)
Chiral HPLC analysis	(page 5)
Construction of ternary isotherm	(page 6)
Thermal analysis (DSC, TG-DTA)	(page 6)
Theoretical calculation	(page 7)
Enantio-enrichment by repeated crystallization	(page 9)
Enantioselective dissolution	(page 10)
Reference	(page 11)

## General remarks

All reagents and solvents were used as received from commercial suppliers.  $^1\text{H}$  NMR spectra were recorded on a Bruker AV400M (400 MHz) spectrometer. The chemical shift of Tetramethylsilane (TMS) or chloroform was used as internal standards for the measurement:  $\delta = 0.00$  or  $7.26$ . Powder X-ray diffraction pattern was collected with Rigaku MiniFlex600. Differential scanning calorimetry (DSC) measurement was conducted with Rigaku Thermo plus EVO2 DSCvesta.

## Synthesis of *rac*-4-cyano-1-aminoindane (**1**)

With a slight modification on the procedure reported by Uthoff and coworkers, *rac*-4-cyano-1-aminoindane (*rac*-**1**) was synthesized as shown in Scheme S1. The modifications were made in the synthesis of **5**, **6**, and **1** to achieve gram-scale synthesis.



Scheme S1. Synthesis of *rac*-**1**.

## Synthesis of **5**

To a 500 mL three-necked flask, equipped with mechanical stirrer and gas release tube, was added **4** (7.92 g, 40.8 mmol), sodium chloride (2.53 g, 43.3 mmol), and clashed aluminum (III) chloride (30.2 g, 226 mmol) and heated to 160 °C for 2 h. 12 M hydrochloric acid (80 mL) and ice (40.0 g) was added, and after stirring for 24 hours, a black solid (5.96 g, 33.7 mmol, 83%) was collected by suction filtration. The black solid was dissolved in methanol (250 mL), activated carbon (12.5 g) was added and refluxed for 90 min. The activated carbon was removed by Celite filtration, and the filtrate was evaporated under reduced pressure to afford the light yellow solid **5** (3.88 g, 220 mmol, 54%).  $^1\text{H}$  NMR (400 MHz, DMSO-*d*<sub>6</sub>):  $\delta$  8.20 (dd,  $J = 7.6$  Hz, 1H), 7.86 (dd,  $J = 7.5$  Hz, 1H), 7.54 (t,  $J = 7.5$  Hz, 1H), 3.38 (m, 2H), 2.64 (m, 2H).

### Synthesis of 6

To the solution of **5** (5.01 g, 28.4 mmol) and triethylamine (13.5 mL, 137 mmol) in tetrahydrofuran (125 mL) at 0 °C, ethyl chloroformate (13.6 mL, 137 mmol) was added and stirred for 1 h. To the reaction mixture was added 28% aqueous ammonia (50 mL, 741 mmol), the mixture was heated to 60 °C, and stirred at room temperature for 4 h. The saturated NaHCO<sub>3</sub> solution was added to quench the reaction, then organic layer was evaporated under vacuum. The mixture was extracted with dichloromethane (100 mL) three times, and the organic phase was washed with saturated brine and dried over MgSO<sub>4</sub>. The solvent was removed under reduced pressure to afford a brown solid (4.02 g, 23.0 mmol, 81%). The crude material included ethyl carbamate, and it was removed by sublimation at 110 °C under reduced pressure for 2 h. Almost pure **6** was obtained as brown solid (3.38 g, 19.3 mmol, 68%). <sup>1</sup>H NMR (400 MHz, DMSO-*d*<sub>6</sub>): δ 7.94 (d, *J* = 7.6 Hz, 1H), 7.73 (d, *J* = 7.2 Hz, 1H), 7.49 (t, *J* = 7.6 Hz, 1H), 3.32 (m, 2H), 2.62 (m, 2H).

### Synthesis of 1

To a 100 mL flask was added **7** (996 mg, 6.34 mmol), hydroxylamine chloride (668 mg, 9.61 mmol), water (8 mL), ethanol (8 mL), 0.5 M NaOH solution (20 mL, 12.3 mmol), and the reaction mixture was refluxed for 3 hours. The reaction mixture was cooled in ice water, and the resulting white precipitate was collected by filtration using a membrane filter. The collected solid was dissolved in acetic acid (15 mL), fine zinc powder (2.10 g, 32.1 mmol, Average Particle Size 6–9 μm, FUJIFILM Wako) was added, and the mixture was stirred at room temperature under a nitrogen atmosphere for 65 hours. The zinc was then removed by Celite filtration. The solid remaining on the Celite was washed with ethyl acetate, and the washing liquid was combined with the filtrate and distilled off under reduced pressure. The resulting solid was dissolved in ethyl acetate (33 mL) and extracted three times with 2 M hydrochloric acid (33 mL). To the acidic aqueous phase, 4 M NaOH solution was added until pH become to 10, and the extraction was carried out using ethyl acetate. The organic phase was washed with saturated brine and dried over MgSO<sub>4</sub>. The solvent was removed under reduced pressure to afford the brown waxy to oily material **1** (343 mg, 2.17 mmol, 35%). <sup>1</sup>H NMR (400 MHz, CDCl<sub>3</sub>): δ 7.64 (d, *J* = 7.5 Hz, 1H), 7.50 (d, *J* = 7.8 Hz, 1H), 7.33 (t, *J* = 7.5 Hz, 2H), 4.36 (t, *J* = 7.3 Hz, 1H), 3.27 (m, 1H), 3.11 (m, 1H), 2.92 (m, 1H), 2.52 (m, 1H), 1.80 (m, 1H).

### Single crystal X-ray diffraction

X-ray diffraction data were collected using a Rigaku XtaLAB P200 diffractometer, and the Mo-*K*α line ( $\lambda = 0.71076 \text{ \AA}$ ) was used as the X-ray source. The data collection was carried out with Rigaku CrystalClear software. The cell refinement and data reduction were carried out with Crysalis PRO.<sup>[S1]</sup> The crystal structure were solved by direct methods using SHELXT<sup>[S2]</sup> and

refined on  $F^2$  with all data using SHELXL-2014.<sup>[S3]</sup> All non-hydrogen atoms were refined anisotropically, and hydrogen atoms were placed in ideal positions and refined as rigid atoms with the relative isotropic displacement parameters. All calculations were carried out using Olex2 program.<sup>[S4]</sup> The programs Mercury were used for analysis and visualization.<sup>[S5]</sup> CCDC deposition number 2236669 contain the supplementary crystallographic data for this paper. These data are provided free of charge by The Cambridge Crystallographic Data Centre.

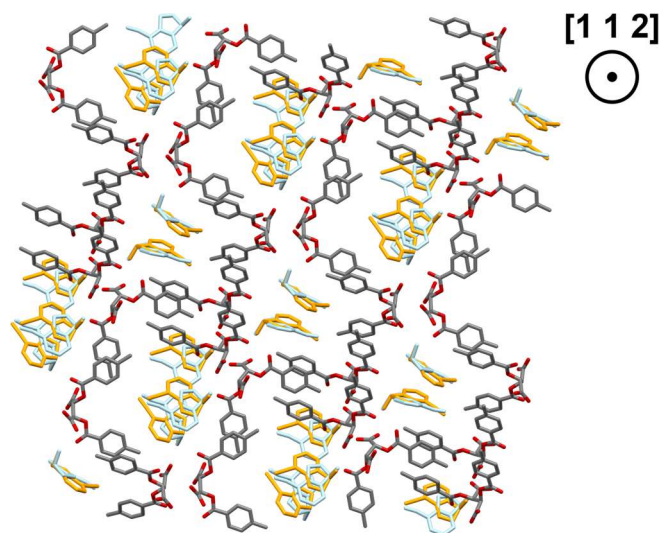


Figure S1. Packing structures of SL salt view along  $[1\ 1\ 2]$  direction. Amine molecules are arrayed on the  $(1\ 1\ 2)$  plane.

Table S1. Crystallographic data of SL.

	SL
Chemical formula	$C_{20}H_{17}O_8, C_{10}H_{11}N_2$
Formula mass	544.54
Crystal system	Orthorhombic
Space group	$C22_1$
$a/\text{\AA}$	7.9768(2)
$b/\text{\AA}$	29.4996(6)
$c/\text{\AA}$	23.6631(5)
Unit cell volume/ $\text{\AA}^3$	5568.2(2)
Temperature/ $^\circ\text{C}$	-113(2)
No. of formula units per unit cell, $Z$	8
No. of measured reflections	67946
No. of independent reflections	7630
$R_{\text{int}}$	0.0968
Final $R_1$ values ( $I > 2\sigma(I)$ )	0.0713
Final $wR(F^2)$ values ( $I > 2\sigma(I)$ )	0.1557
Final $R_1$ values (all data)	0.0963
Final $wR(F^2)$ values (all data)	0.1664
Goodness of fit on $F^2$	1.051

### Chiral HPLC analysis

The accurate chiral composition of **1** in solid samples was determined by using high-performance liquid chromatography (HPLC) with CROWNPAK CR-I (+) column (DICEL CORPORATION,  $\phi 3.0 \times 150 \text{ mm} \times 5 \mu\text{m}$ ) employing a mixture of acetonitrile and aqueous solution of  $\text{HClO}_4$  (pH = 1.5) (2/8, v/v) as the mobile phase at the flow rate of 0.7 mL/min. The wavelength employed for UV detection was 230 nm. The column oven was used to maintain the temperature of column at 7 °C. Preliminary test was conducted using SUMICHIRAL OA-8000 column (Sumika Chemical Analysis Service, Ltd.,  $\phi 4.6 \times 250 \text{ mm} \times 5 \mu\text{m}$ ) with a circular dichroism detector at 230 nm. All analyses were performed using a JASCO HPLC system (PU-2089 AS-2055i, UV-2075, CD-2095, CO-2060 and LC-NET II/ADC).

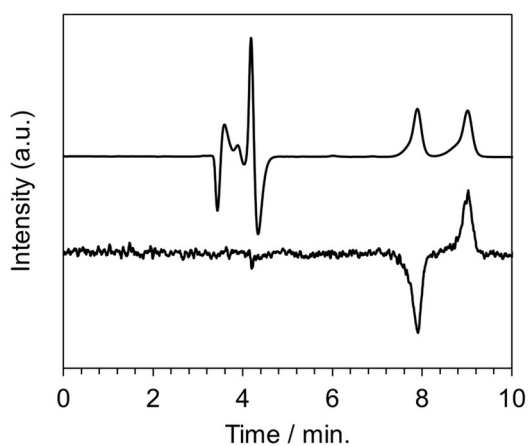


Figure S2. HPLC chromatograms of *rac*-**1** using SUMICHIRAL OA-8000 column. Upper trace is obtained with UV detector at 280 nm, bottom trace is obtained with CD detector at 280 nm.

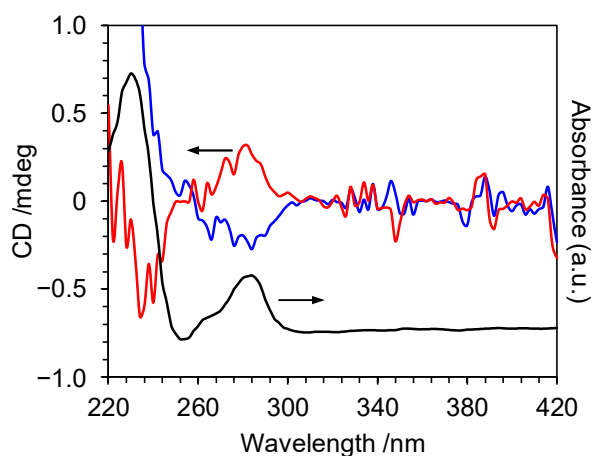


Figure S3. Circular dichroism and UV spectra of **1**. Both spectra were recorded with CD detector.

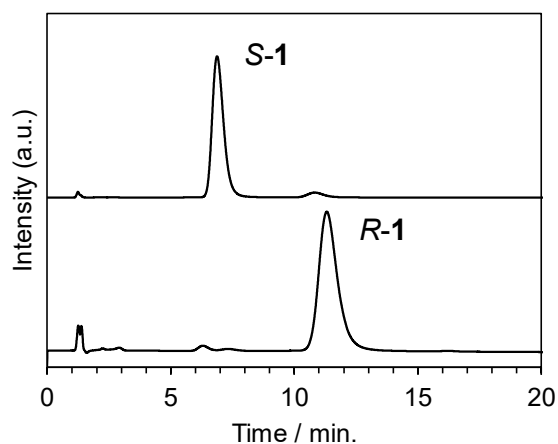


Figure S4. HPLC chromatograms of *S-1* and *R-1* with CROWNPAK CR-I(+) column.

### Construction of ternary isotherm

The suspension of crystals in methanol controlled at 20 °C and stirred for 24 h. After stirring was stopped, part of the crystalline phase was collected by filtration and dried, the crystalline phase was confirmed by PXRD and *ee* of **1** in the crystal was determined by HPLC analysis. In the SL/RL/MeOH ternary isotherm, the composition of the saturated supernatant was plotted as a solubility curve and the corresponding composition of the crystalline phase was connected by tie lines.

### Thermal analysis (DSC, TG-DTA)

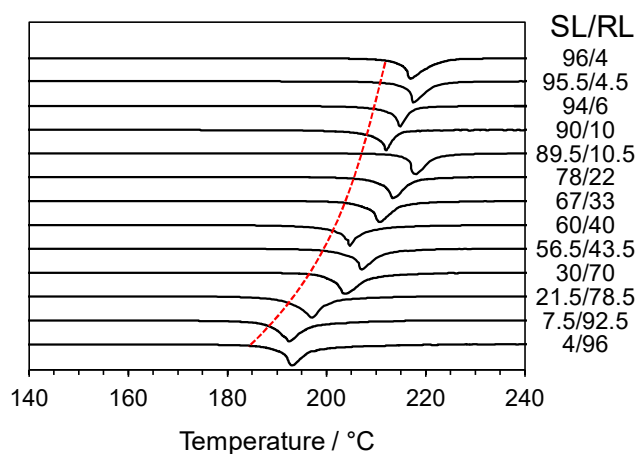


Figure S5. DSC melting endotherms of crystalline samples with various composition upon heating at 5 K/min. The compositions are indicated on the right side.

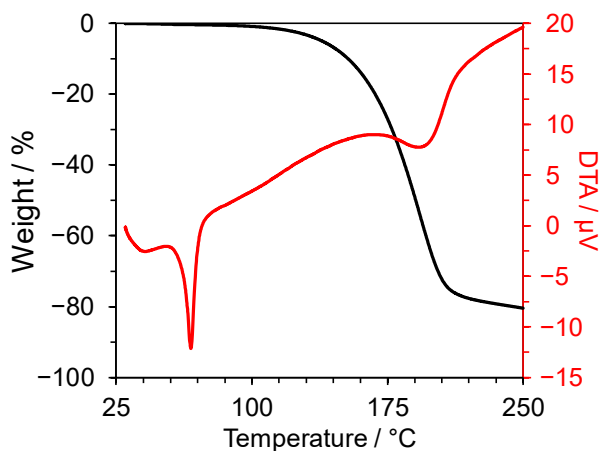


Figure S6. TG-DTA chart of *rac-1*. The black line indicate TG profile, and the red line indicate DTA curve. Heating rate is 5 K min<sup>-1</sup>. N<sub>2</sub> flow is 100 mL min<sup>-1</sup>.

### Theoretical calculation

Optimization of hydrogen position in the experimentally obtained crystal structure of **SL** was carried out with dispersion force corrected DFT method using periodic boundary condition on Quantum ESPRESSO 5.2.1 software.<sup>[S6-8]</sup> The Winmostar program was used as GUI.<sup>[S9]</sup> PBE functional with Grimme's dispersion correction method (D3 method) was used. The PSlibrary's ultrasoft pseudopotentials for PBE functional were used for all elements.<sup>[S10]</sup> The cutoff for wavefunctions (ecutwfc) and charge density (ecutrho) were gradually tightened, and the cutoff energy used in the final optimization were 64 and 576 Ry, respectively. The conversion threshold on total energy and forces for ionic minimization was used default value, 1.0D-4 and 1.0D-3, respectively. The conversion threshold for self-consistency calculation was 1.0D-8. K points was set at the gamma position except for the final optimization, and 3×3×3 was used in the final optimization. The geometry of **RL** were generated by replacing *S*-isomer with *R*-isomer and optimized as same procedure as above.

To investigate the stabilization energy, intermolecular interaction energies between *S*- or *R*-isomer and surrounding molecules were calculated. The surrounding molecules are selected based on the short contact on Mercury software. The charge of amine molecules is set as +1. The charge of carboxylic acids were set as 0 or -1. The calculation of the intermolecular interaction energies was conducted on one surrounding molecule and single *S*- or *R*-isomer. The total intermolecular interaction energies were calculated at the MP2/aug-cc-pVDZ level of theory using Gaussian16 software.<sup>[S11]</sup> The basis set superposition error (BSSE) was corrected by the counterpoise method. HF level interaction energy ( $E_{HF}$ ) was calculated using the aug-cc-pVDZ basis set. GDMA program (version 2.3.3)<sup>[S12]</sup> was used to calculate distributed multipole of isolated molecules on all atoms up to hexadecapole using wave functions of MP2/aug-cc-pVDZ level. ORIENT

program (version 5.0.11) <sup>[S13]</sup> was used to calculate electrostatic interaction energy ( $E_{es}$ ) and induction energy ( $E_{ind}$ ) based on atomic polarizabilities and the electronic field obtained by the distributed multipoles. As the electron correlation in the neutral organic molecules was mainly dispersion interaction, dispersion interaction energy ( $E_{disp}$ ) was calculated taking difference between estimated energy using MP2 and HF methods, namely  $E_{disp} = E_{int} - E_{HF}$ . The short-range interaction ( $E_{short}$ ), exchange-repulsion and charge-transfer, was calculated as difference between  $E_{HF}$ , and sum of  $E_{es}$  and  $E_{ind}$ , namely  $E_{short} = E_{HF} - E_{es} - E_{ind}$ .

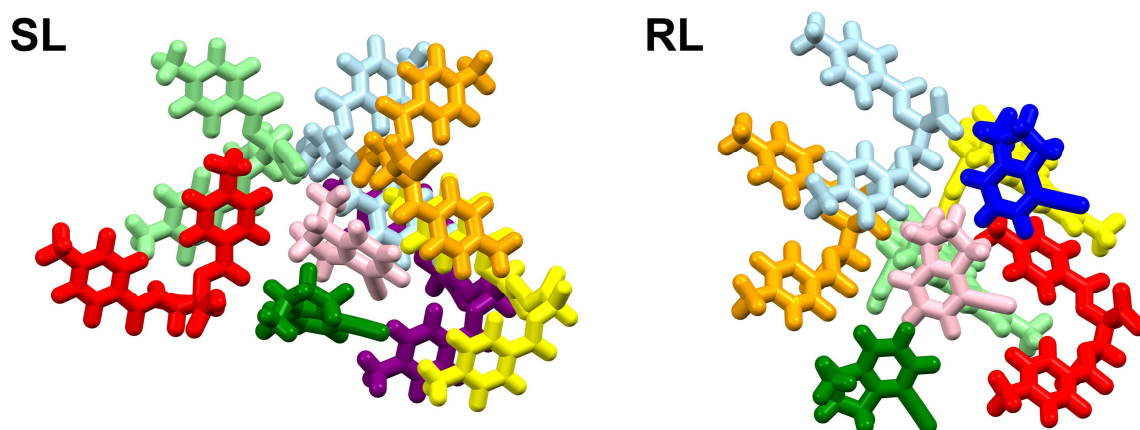
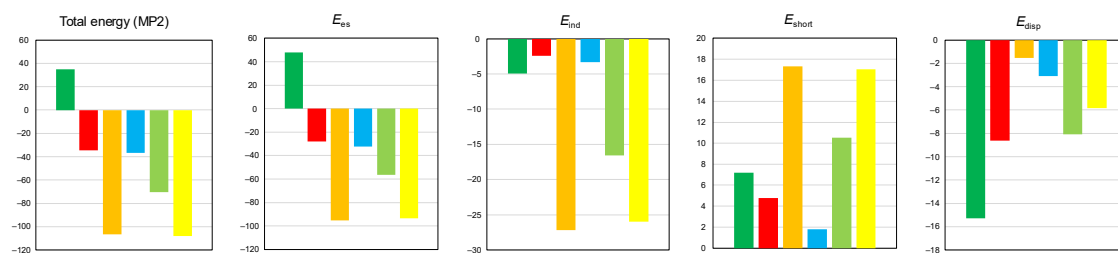


Figure S7. The geometries of **SL** and **RL** for the calculation of intermolecular interaction energies. The amine molecule (pink) is focused as center molecule. All the calculation was conducted against this molecule.

(a) Intermolecular interaction energies between S-1 and surrounding molecules (kcal mol<sup>-1</sup>)



(b) Intermolecular interaction energies between R-1 and surrounding molecules (kcal mol<sup>-1</sup>)

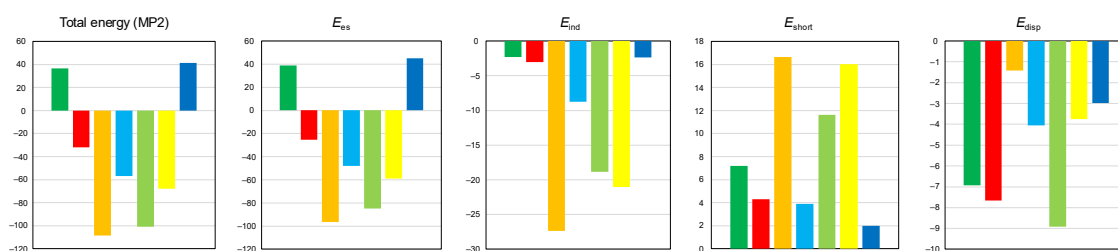


Figure S8. Intermolecular interaction energies against the amine molecule (a) in the **SL**, and (b) **RL** crystals. The color bars correspond to the molecular color used in Figure S7.

The total intermolecular interaction energies are favorable for amine molecules in both of **SL** and **RL** crystals. The electrostatic energy is the most dominant attraction force between amine and carboxylic acids. The sum of the total intermolecular interaction energies for *S*-**1** and carboxylic acids is  $-320 \text{ kcal mol}^{-1}$ , and for *R*-**1** is  $-309 \text{ kcal mol}^{-1}$ . The interaction energies with adjacent amine molecule are repulsive because of large electrostatic energy between cations. However, the dispersion energies work as attractive force, and *S*-**1** receive stronger stabilization energy than **RL**. These calculations can describe that **SL** is favorable crystal structure in terms of intermolecular interactions in the crystal structure.

### Enantio-enrichment by repeated crystallization

The crystalline sample of *rac*-**1** and L-acid (800 mg) was suspended in methanol (15 mL) and stirred for 1 day, then collected crystals by filtration. The *ee* of **1** in the collected crystals was analyzed by HPLC and then stirred in methanol for 1 day. This process was repeated five times to confirm the crystallization behavior and reproducibility of isotherm.

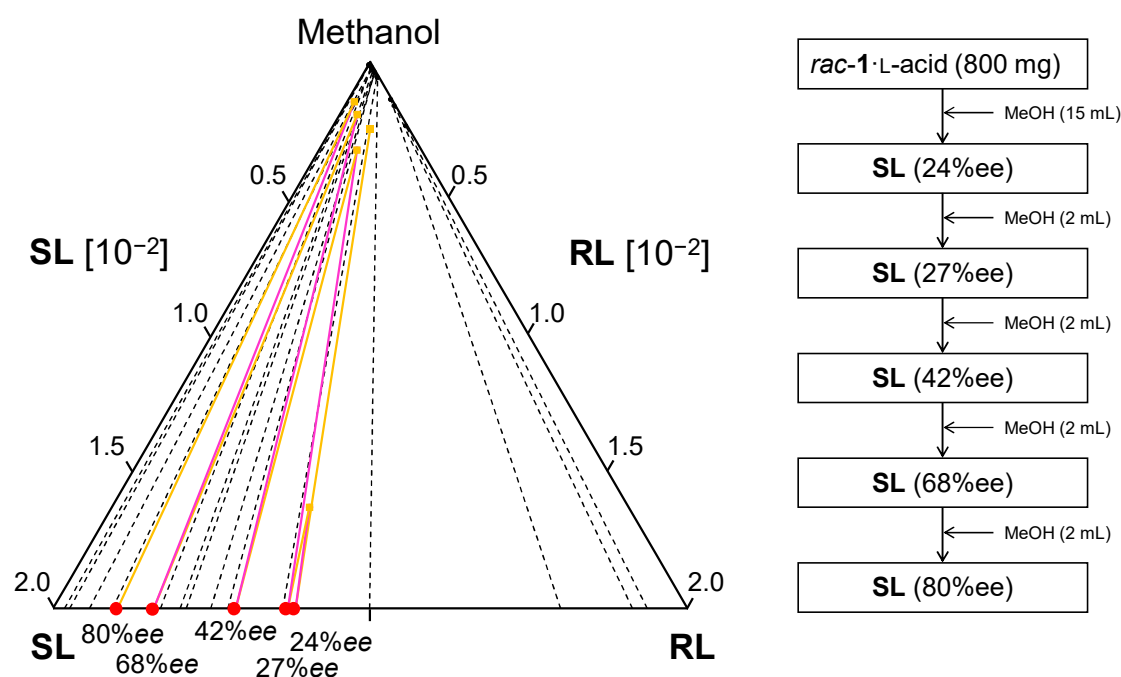


Figure S9. Chiral enrichment of **SL** by crystallization in methanol. The suspension reached at thermodynamical equilibrium. Orange rectangle symbols indicate the initial composition of crystallization. Orange lines represent crystallization pathway. Red circle symbols on the bottom line indicate *ee* of **1** in the resulting crystals. Red lines indicate the change of composition by adding methanol.

### Enantioselective dissolution

The crystalline samples with different *ee* were prepared by repeated crystallization. About 20 mg of crystals are stirred in the methanol at 50 °C for 5 min. After dissolution, the crystals were collected by filtration and dried *in vacuo*. After weighing the collected crystal, the *ee* of **1** in the crystal was determined by HPLC analysis.

To investigate appropriate duration of dissolution, the time course of enantiomeric excess of **1** in the crystal during dissolution in methanol was recorded (Figure S6). The crystalline sample with 24%*ee* were used for the experiment. The *ee* of **1** in the crystal increased to 40% in the initial 5 min, and gradually increased over 150 min. Since the rapid increase of *ee* was observed in the 5 min, the duration of dissolution was set as 5 min.

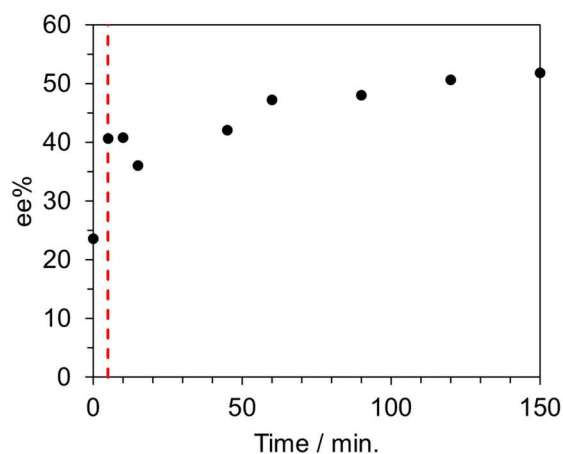


Figure S10. Time course of enantiomeric excess (*ee*) of *S*-**1**-L-acid in the methanol at 50 °C. Red dash line indicates at the time of 5 min.

Table S2. Summary of enantioselective dissolution experiments.

Run	Initial <i>ee</i> of <b>1</b> in the solid	Collected mass / mg	Final <i>ee</i> of <b>1</b> in the solid
1	23.6	14.0	40.7
2	41.4	14.1	56.3
3	56.9	13.3	68.4
4	61.3	16.0	69.4
5	88.4	15.6	90.4
6	92.3	15.3	96.1
7	-51.8	5.31	-3.0

## Reference

- [S1] Agilent CrysAlis PRO. Agilent Technologies Ltd, Yarnton, Oxfordshire, England, 2014.
- [S2] G. M. Sheldrick, *Acta Crystallogr. Sect. A Found. Adv.* 2015, **71**, 3.
- [S3] G. M. Sheldrick, *Acta Crystallogr. Sect. C Struct. Chem.* 2015, **71**, 3.
- [S4] O. V. Dolomanov, L. J. Bourhis, R. J. Gildea, J. A. K. Howard, H. Puschmann, *J. Appl. Crystallogr.* 2009, **42**, 339.
- [S5] C. F. Macrae, I. Sovago, S. J. Cottrell, P. T. A. Galek, P. McCabe, E. Pidcock, M. Platings, G. P. Shields, J. S. Stevens, M. Towler, P. A. Wood, *J. Appl. Crystallogr.* 2020, **53**, 226.
- [S6] P. Giannozzi, S. Baroni, N. Bonini, M. Calandra, R. Car, C. Cavazzoni, D. Ceresoli, G. L. Chiarotti, M. Cococcioni, I. Dabo, A. Dal Corso, S. de Gironcoli, S. Fabris, G. Fratesi, R. Gebauer, U. Gerstmann, C. Gougoussis, A. Kokalj, M. Lazzeri, L. Martin-Samos, N. Marzari, F. Mauri, R. Mazzarello, S. Paolini, A. Pasquarello, L. Paulatto, C. Sbraccia, S. Scandolo, G. Sclauzero, A. P. Seitsonen, A. Smogunov, P. Umari, R. M. Wentzcovitch, *J. Phys. Condens. Matter* 2009, **21**, 395502.
- [S7] P. Giannozzi, O. Andreussi, T. Brumme, O. Bunau, M. Buongiorno Nardelli, M. Calandra, R. Car, C. Cavazzoni, D. Ceresoli, M. Cococcioni, N. Colonna, I. Carnimeo, A. Dal Corso, S. de Gironcoli, P. Delugas, R. A. DiStasio, A. Ferretti, A. Floris, G. Fratesi, G. Fugallo, R. Gebauer, U. Gerstmann, F. Giustino, T. Gorni, J. Jia, M. Kawamura, H.-Y. Ko, A. Kokalj, E. Küçükbenli, M. Lazzeri, M. Marsili, N. Marzari, F. Mauri, N. L. Nguyen, H.-V. Nguyen, A. Otero-de-la-Roza, L. Paulatto, S. Poncé, D. Rocca, R. Sabatini, B. Santra, M. Schlipf, A. P. Seitsonen, A. Smogunov, I. Timrov, T. Thonhauser, P. Umari, N. Vast, X. Wu, S. Baroni, *J. Phys. Condens. Matter* 2017, **29**, 465901.
- [S8] P. Giannozzi, O. Baseggio, P. Bonfà, D. Brunato, R. Car, I. Carnimeo, C. Cavazzoni, S. de Gironcoli, P. Delugas, F. Ferrari Ruffino, A. Ferretti, N. Marzari, I. Timrov, A. Urru, S. Baroni, *J. Chem. Phys.* 2020, **152**, 154105.
- [S9] *Winmostar VII.3.1*, X-Ability Co. Ltd., Tokyo, Japan, 2022.
- [S10] A. Dal Corso, *Comput. Mater. Sci.* 2014, **95**, 337.
- [S11] *Gaussian 16, Revision C.01*, M. J. Frisch, G. W. Trucks, H. B. Schlegel, G. E. Scuseria, M. A. Robb, J. R. Cheeseman, G. Scalmani, V. Barone, G. A. Petersson, H. Nakatsuji, X. Li, M. Caricato, A. V. Marenich, J. Bloino, B. G. Janesko, R. Gomperts, B. Mennucci, H. P. Hratchian, J. V. Ortiz, A. F. Izmaylov, J. L. Sonnenberg, D. Williams-Young, F. Ding, F. Lipparini, F. Egidi, J. Goings, B. Peng, A. Petrone, T. Henderson, D. Ranasinghe, V. G. Zakrzewski, J. Gao, N. Rega, G. Zheng, W. Liang, M. Hada, M. Ehara, K. Toyota, R. Fukuda, J. Hasegawa, M. Ishida, T. Nakajima, Y. Honda, O. Kitao, H. Nakai, T. Vreven, K. Throssell, J. A. Montgomery, Jr., J. E. Peralta, F. Ogliaro, M. J. Bearpark, J. J. Heyd, E. N. Brothers, K. N. Kudin, V. N. Staroverov, T. A. Keith, R. Kobayashi, J. Normand, K. Raghavachari, A. P. Rendell, J. C. Burant, S. S. Iyengar, J. Tomasi, M. Cossi, J. M. Millam, M. Klene, C. Adamo, R. Cammi, J. W. Ochterski, R. L. Martin, K. Morokuma, O. Farkas, J. B. Foresman and D. J. Fox, Gaussian, Inc., Wallingford CT, 2019.
- [S12] A. J. Stone, *J. Chem. Theory Comput.* 2005, **1**, 1128.
- [S13] *Orient, version 5.0*, A. J. Stone, A. Dullweber, O. Engkvist, E. Frascini, M. P. Hodges, A. W. Meredith, D. R. Nutt, P. L. A. Popelier, and D. J. Wales, 2018